

Microstructure and Properties of Spark Plasma Sintered Al–Zn–Mg–Cu Alloy

H. BECKER^{a,*}, M. DOPITA^a, J. STRÁSKÁ^b, P. MÁLEK^b, M. VILÉMOVÁ^c AND D. RAFAJA^a

^aInstitute of Materials Science, TU Bergakademie Freiberg, 09599 Freiberg, Germany

^bCharles University in Prague, Department of Physics of Materials, Prague, Czech Republic

^cAcademy of Sciences of the Czech Republic, Institute of Plasma Physics, Prague, Czech Republic

The microstructure of an aluminum alloy containing 53 wt% Zn, 2.1 wt% Mg and 1.3 wt% Cu as main alloying elements has been studied with the focus on the precipitation behavior during the spark plasma sintering process. The starting material was an atomized Al–Zn–Mg–Cu powder with the particle size below 50 μm . The particles showed a solidification microstructure from cellular to columnar or equiaxed dendritic morphology with a large fraction of the alloying elements segregated in form of intermetallic phases, mainly $(\text{Zn,Al,Cu})_{49}\text{Mg}_{32}$ and $\text{Mg}_2(\text{Zn,Al,Cu})_{11}$, at the cell and dendrite boundaries. The microstructure of the sintered specimens followed the microstructure of the initial powder. However, $\text{Mg}(\text{Zn,Al,Cu})_2$ precipitates evolve at the expense of the initial precipitate phases. The precipitates which were initially continuously distributed along the intercellular and interdendritic boundaries form discrete chain-like structures in the sintered samples. Additionally, fine precipitates created during the sintering process evolve at the new low-angle boundaries. The large fraction of precipitates at the grain boundaries and especially at the former particle boundaries could not be solved into the matrix applying a usual solid solution heat treatment. A bending test reveals low ductility and strength. The mechanical properties suffer from the precipitates at former particle boundaries leading to fracture after an outer fiber tensile strain of 3.8%.

DOI: [10.12693/APhysPolA.128.602](https://doi.org/10.12693/APhysPolA.128.602)

PACS: 81.05.Bx, 81.20.Fw, 81.40.-z, 81.70.-q, 61.43.Gt, 81.20.Ev, 62.20.M-

1. Introduction

Lightweight Al–Zn–Mg–Cu alloys are used for their high strength and ductility in various industrial applications. As their mechanical properties strongly depend on the precipitation characteristics, the microstructure of the Al–Zn–Mg–Cu alloys can be optimized following the precipitation sequence: supersaturated solid solution (SSSS) \rightarrow Guinier Preston zones (GP I, II) \rightarrow η' -phase \rightarrow ηMgZn_2 [1, 2]. This precipitation sequence is provided when nucleation occurs homogeneously. Additionally, the precipitation of η' -phase and ηMgZn_2 occurs preferentially heterogeneously at grain boundaries and microstructure defects as dislocations which are induced by material processing that involves plastic deformation [3–5]. However, for high strength and high ductility a microstructure containing fine GP and coarser η' -precipitates in the grain interior is favourable [6, 7]. Consequently, a T6 heat treatment consisting of a solid solution treatment, usually for 1 h at 470 to 500 °C and subsequent quenching in water is applied to form a solid solution and annihilate the dislocations [3, 7, 8]. It is followed by a controlled ageing step during which new precipitates form in the grain interior [1, 2, 4, 7, 8]. The ageing time and temperature influence the chemical and phase composition as well as the quantity and size of the precipitates [1, 9].

Figure 1 shows the basic development of the precipitations starting from the initial SSSS. The phase fields of the intermetallics are very narrow in the low alloy content range, thus also $\text{Mg}_2\text{Zn}_{11}$ and $(\text{Al,Zn})_{49}\text{Mg}_{32}$ can occur next to ηMgZn_2 [10]. In the Al–Zn–Cu–Mg system, the intermetallic phases form an isomorph series with the intermetallic phases known from the Al–Zn–Mg system; Zn is partially substituted by Cu: $\text{Mg}(\text{Zn,Al,Cu})_2$ ($P6_3/mmc$), $(\text{Zn,Al,Cu})_{49}\text{Mg}_{32}$ ($Im-3$) and $\text{Mg}_2(\text{Zn,Al,Cu})_{11}$ ($Pm-3$) [11–13]. In order to investigate the precipitation behavior in samples prepared using the spark plasma sintering technique, an Al–Zn–Mg–Cu alloy powder was compacted and the microstructure evolution and mechanical properties were studied.

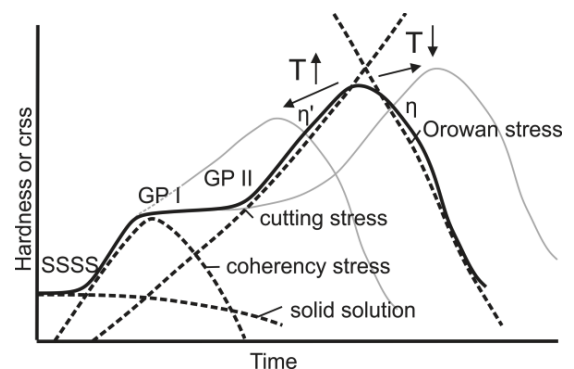


Fig. 1. Schematic precipitation sequence in the Al–Zn–Mg–Cu alloys related to the hardness or critical resolved shear stress (crss) as a function of time and temperature [1, 9].

*corresponding author; e-mail:

Hanka.Becker@iw.tu-freiberg.de

2. Experimental details

The Al–Zn–Mg–Cu powder was atomized in an Ar stream. The sieved powder with particle sizes below $50\ \mu\text{m}$ was used for further experiments. The powder composition is given in the Table. The powder was compacted using the spark plasma sintering/field assisted sintering technology (SPS/FAST) device FCT SPS-HP25 (FCT Systeme GmbH). The sintering was done in vacuum at the load on the piston of 80 MPa. The sintering temperatures ranged between 698 K and 823 K. The standard sintering time was 3 min. Additional samples were sintered at 698 K and 748 K for 20 min. One specimen sintered at 823 K for 3 min was subsequently annealed in vacuum for 1 h at 743 K and quenched into water in order to examine the influence of longer sintering or annealing times on the precipitations.

The cross-sections of the sintered and annealed samples were ground and polished down to colloidal silica suspension. The morphology and microstructure of the specimens were investigated using the high-resolution field-emission scanning electron microscope (SEM) LEO 1530 (Carl Zeiss). It was equipped with a Nordlys II (Oxford Instruments) detector for electron backscattered diffraction (EBSD) measurement. The HKL Channel 5 software (Oxford Instruments) was used for pattern acquisition and indexing. To study the fine details of the sample microstructure scanning transmission electron microscopy (STEM) was done on a 200 kV analytical high-resolution transmission electron microscope JEM 2010 FEF (JEOL). To obtain information about the phase composition X-ray diffraction (XRD) measurements were carried out on a conventional para-focusing Bragg-Brentano diffractometer URD-6 (from Seifert/Freiburger Präzisionsmechanik), which was equipped with a sealed X-ray tube with Cu anode and a graphite monochromator in the diffracted beam. A four point bending test was performed to correlate the microstructure with the mechanical properties of specimens.

TABLE

Overall chemical composition of the Al–Zn–Mg–Cu alloy determined using the SEM/EDX averaged over a sample area of $80 \times 60\ \mu\text{m}^2$.

Element	Zn	Mg	Cu	Fe	Si	Al
weight%	5.31 ± 0.2	2.09 ± 0.2	1.34 ± 0.05	0.4 ± 0.02	0.65 ± 0.05	balance

3. Results and discussion

3.1. Microstructure evolution

The spherical particles of atomized Al–Zn–Mg–Cu powder show a solidification microstructure from cellular to columnar or equiaxed dendritic with a large fraction of the alloying elements continuously segregated in form of intermetallic phases at the cell, column and dendrite boundaries (Fig. 2). The boundary regions consist mainly of $(\text{Zn,Al,Cu})_{49}\text{Mg}_{32}$ with a low fraction of $\text{Mg}_2(\text{Zn,Al,Cu})_{11}$ as identified by XRD (Fig. 3b). Additionally, $\text{Al}_{13}\text{Fe}_4$, $\text{Al}_7\text{Cu}_4\text{Fe}$, and Mg_2Si precipitates were

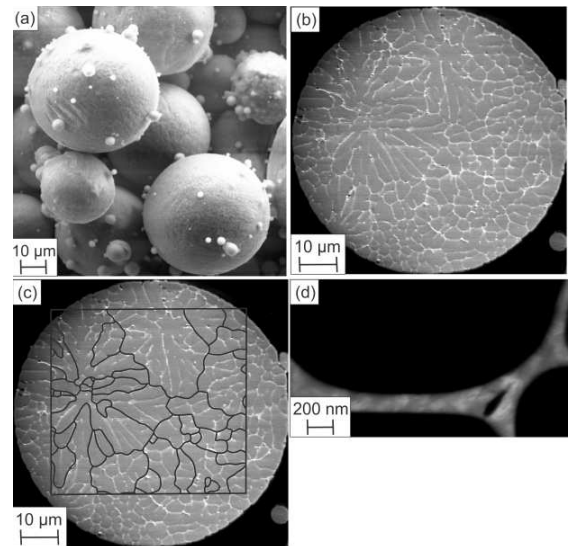


Fig. 2. SEM micrographs of atomized Al–Zn–Mg–Cu powder, (a) secondary electron (SE) contrast of the spherical powder particles (b) backscattered electron (BSE) contrast of a particle crosssection showing the cellular to columnar or equiaxed dendritic morphology whose dimensions are indicated by the black lines in (c). The continuous segregation of the alloying elements is highlighted in part (d).

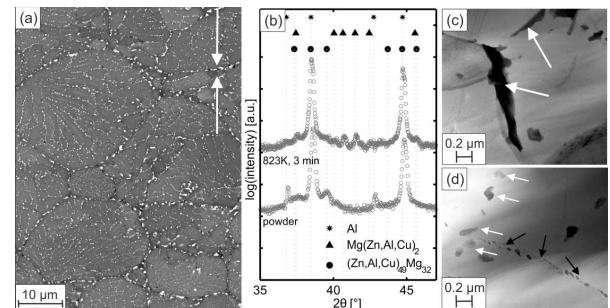


Fig. 3. (a) SEM/BSE micrograph of the sample sintered at 823 K for 3 min. The pressure application direction during SPS is indicated by the white arrows. (b) 2θ sections from 35° to 47° of the XRD patterns showing the phase evolution of dominant precipitation phases (c) STEM micrograph showing high angle boundary precipitates (white arrows), (d) STEM micrograph with precipitates evolved from segregation regions with the same crystallographic orientation on both sides of initially continuous segregation (white arrows) and small angle boundary precipitates (black arrows).

found as a consequence of impurity elements Fe and Si in the starting powder.

The morphology and microstructure of sintered specimens follow the microstructure of the powder. The precipitates, which were initially continuously segregated along the intercellular or -dendritic boundary regions (Fig. 2b–d), form discrete, chain-like structures in the sintered samples (Fig. 3a). In addition to the precipitates in the powder, the fraction of $(\text{Zn,Al,Cu})_{49}\text{Mg}_{32}$ decreased at the expense of $\text{Mg}(\text{Zn,Al,Cu})_2$, which evolved

in the sintered specimens (Fig. 3b). The impurity phases remained unchanged. The precipitates at the former particle surfaces and between grains are lens-shaped and larger (approximately $1\ \mu\text{m}$ in longer direction) than the precipitates (approximately 150 to 200 nm), which evolve from the segregation regions where the same crystallographic orientation was on both sides of the initially continuous segregation (Fig. 3c,d). After sintering, the grains have a mean size of approximately $6\ \mu\text{m}$ in the direction of the applied pressure and approximately $7.5\ \mu\text{m}$ in the perpendicular direction. Accordingly, the deformation induced by the loading during SPS leads to a weak sintering $\langle 110 \rangle$ texture, which is in agreement to the compression texture in fcc metals [14]. The generated dislocations form low angle boundaries $< 5^\circ$, which act as preferential heterogeneous nucleation sites for arrays of very small $< 50\ \text{nm}$ precipitates (Fig. 3d). This finding is in a good agreement with results published in [4, 5]. A similar microstructure was also observed in the samples, which were SPS sintered for 20 min, and in the SPS samples, which were annealed in vacuum and quenched in water. Mondal and Mukhopadhyay [12] reported that the solubility is very sensitive to the alloy composition in Al–Zn–Mg–Cu as the phase fields are very narrow in the low alloy range ($< 5\ \text{at.}\% \text{ Zn}$, $< 5\ \text{at.}\% \text{ Mg}$, $< 5\ \text{at.}\% \text{ Cu}$) [10]. Depending on the exact chemical composition the precipitates cannot be solved [15] or it takes longer than 24 h to form a solid solution [12, 16]. The precipitates containing the impurity elements Si and Fe are stable to higher temperatures than the applied heat treatment temperatures [16, 17].

3.2. Mechanical properties and observation of the deformation mechanism

The bending test revealed a 0.2% yield strength of about 150 MPa which is extremely low in comparison to the optimized microstructural state [7]. It is comprehensible because the microstructure under investigation is comparable to the microstructure received at the long time region of the curve in Fig. 1. The bending

leads to the fracture already after an outer fiber tensile strain of 3.8% at an outer fiber tensile stress of approximately 300 MPa. The fracture surface and the outer fiber tensile surface show that the failure occurred preferentially between the former powder particles where the largest precipitates have formed (Fig. 4a,b). The failure at low strains is usually attributed to intermetallic precipitates at grain boundaries [6]. Because the microstructure of the SPS samples changed substantially neither after a “long-time” spark plasma sintering nor after the vacuum heat treatment and the quenching, the mechanical properties of these alternatively treated samples were comparable with the samples subjected to the short-time SPS process.

4. Conclusions

The microstructure of an Al–Zn–Mg–Cu alloy was investigated in the original state as an atomized powder and after compaction using the spark plasma sintering process. In the solidification microstructure of the original state, precipitates with a high content of alloying elements are continuously segregated between the cell, column and dendrite structure. After the spark plasma sintering, chain-like arranged precipitates form, which are arranged along the locations of former segregations. Additionally, favored precipitation at dislocations arranged in low angle boundaries was observed. The sintered samples exhibit low ductility and strength. Especially, the intermetallic precipitates between the initial particles lead to fracture at low strains.

Acknowledgments

Two of the authors, J.S. and M.V., acknowledge financial support by the Grant Agency of the Czech Republic under the grant no. 14-36566G. The authors wish to acknowledge the German Research Foundation (DFG) for supporting the subproject A05, which is a part of the Collaborative Research Centre 920 (CRC 920).

References

- [1] H.K. Hardy, T.J. Heal, *Prog. Met. Phys.* **5**, 143 (1954).
- [2] J.Z. Liu, J.H. Chen, X.B. Yang, S. Ren, C.L. Wu, H.Y. Xub, J. Zoub, *Scr. Mater.* **63**, 1064 (2010).
- [3] T. Hu, K. Ma, T.D. Topping, J.M. Schoenung, E.J. Lavernia, *Acta Mater.* **61**, 2163 (2013).
- [4] J. Gubicza, I. Schiller, N.Q. Chinh, J. Illy, Z. Horita, T.G. Langdon, *Mater. Sci. Eng. A* **460-461**, 77 (2007).
- [5] P.N.T. Unwin, R.B. Nicholson, *Acta Metall.* **17**, 1379 (1969).
- [6] H. Chen, B. Yang, *Mater. Trans.* **49**, 2912 (2008).
- [7] K. Ma, H. Wen, T. Hu, T.D. Topping, D. Isheim, D.N. Seidman, E.J. Lavernia, J.M. Schoenung, *Acta Mater.* **62**, 141 (2014).

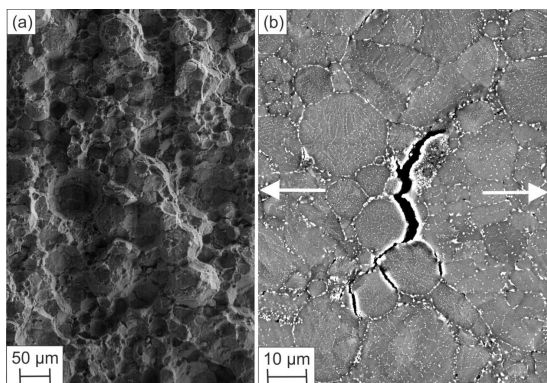


Fig. 4. (a) SEM/SE micrograph of the fracture surface and (b) SEM in BSE contrast showing the crack located between former powder particles. The outer fiber tensile stress direction is indicated by white arrows.

- [8] J.-F. Li, Z.-W. Peng, C.-X. Li, Z.-Q. Jia, W.-J. Chen, Z.Q. Zheng, *Trans. Nonferrous Met. Soc. China***18**, 755 (2008).
- [9] D.R. Askeland, F. Haddleton, P. Green, H. Robertson, in: *The Science and Engineering of Materials*, Chapman and Hall, London 1996, p. 289.
- [10] H. Liang, S.-L. Chen, Y.A. Chang, *Met. Mat. Trans. A* **28A**, 1725 (1997).
- [11] X. Fang, M. Song, K. Li, Y. Du, D. Zhao, C. Jiang, H. Zhang, *J. Mater. Sci.* **47**, 5419 (2012).
- [12] C. Mondal, A.K. Mukhopadhyay, *Mater. Sci. Eng. A* **391**, 367 (2005).
- [13] S. Samson, *Acta Chem. Scand.* **3**, 835 (1949).
- [14] B. Clausen, Ph.D. Thesis, Risø National Laboratory, Roskilde 1997.
- [15] H.-B. Chen, K. Tao, B. Yang, J.-S. Zhang, *Trans. Nonferrous Met. Soc. China* **19**, 1110 (2009).
- [16] X. Fan, D. Jiang, Q. Meng, L. Zhong, *Mater. Lett.***60**, 1475 (2006).
- [17] F. Xie, X. Yan, L. Ding, F. Zhang, S. Chen, M.G. Chu, Y.A. Chang, *Mater. Sci. Eng. A* **355**, 144 (2003).